Journal of Physics D: Applied Physics

PAPER • **OPEN ACCESS**

Improving SPLIT-STED super-resolution imaging with tunable depletion and excitation power

To cite this article: Simone Pelicci *et al* 2020 *J. Phys. D: Appl. Phys.* **53** 234003

View the article online for updates and enhancements.

IOP ebooks™

Bringing together innovative digital publishing with leading authors from the global scientific community.

Start exploring the collection–download the first chapter of every title for free.

This content was downloaded from IP address 93.37.176.225 on 08/04/2020 at 09:03

OPEN ACCESS
IOP Publishing
Journal of Physics D: Applied Physics
J. Phys. D: Appl. Phys. **53** (2020) 234003 (12pp)
https://doi.org/10.1088/1361-6463/ab7cf8

Improving SPLIT-STED super-resolution imaging with tunable depletion and excitation power

Simone Pelicci[1,2], Giorgio Tortarolo[3,4], Giuseppe Vicidomini[3], Alberto Diaspro[1,2] and Luca Lanzanò[1,5]

[1] Nanoscopy and Nikon Imaging Center, Istituto Italiano di Tecnologia, Genoa, Italy
[2] Department of Physics, University of Genoa, Genoa, Italy
[3] Molecular Microscopy and Spectroscopy, Istituto Italiano di Tecnologia, Genoa, Italy
[4] Dipartimento di Informatica, Bioingegneria, Robotica e Ingegneria dei Sistemi, University of Genoa, Genoa, Italy

E-mail: luca.lanzano@iit.it and alberto.diaspro@iit.it

Received 15 January 2020, revised 24 February 2020
Accepted for publication 5 March 2020
Published 7 April 2020

Abstract

The SPLIT approach is a simple and efficient way to improve the spatial resolution of a super-resolved STED multi-dimensional image, i.e. a STED image in which an additional dimension encodes spatial information. Recently, we have demonstrated that the SPLIT can be applied to multidimensional STED images obtained with tunable depletion power. In this SPLIT-STED implementation, the additional dimension is represented by the depletion power, a parameter that can be easily tuned on any STED microscope. In this work, we introduce a modified implementation in which we tune also the excitation power. The tuning of the excitation power is used to modulate the number of photons collected for each STED image. We show that the modified SPLIT-STED method produces an improvement of spatial resolution for very different tuning patterns of the excitation intensity, improving the versatility of the SPLIT-STED approach. Interestingly, we find that the extent of photobleaching can be modulated by the excitation pattern, as it depends on the simultaneous impact of high STED and excitation powers. Thus, the tuning of the excitation power can improve applicability of the method to live cell imaging, potentially minimizing the photobleaching of the fluorophores and the phototoxicity on the biological samples during a SPLIT-STED acquisition. We apply the modified SPLIT-STED method to super-resolution imaging of nuclear periphery, in both fixed and live cells.

Supplementary material for this article is available online

Keywords: STED, SPLIT, tunable STED power, tunable excitation power, superresolution, nuclear lamin, phasor anaysis

(Some figures may appear in colour only in the online journal)

[5] Present address: Department of Physics and Astronomy 'Ettore Majorana', University of Catania, Catania, Italy

Original content from this work may be used under the terms of the Creative Commons Attribution 4.0 licence. Any further distribution of this work must maintain attribution to the author(s) and the title of the work, journal citation and DOI.

1. Introduction

The eukaryotic cell nucleus is characterized by different heterogeneous biological structures, such as the nuclear envelope (NE) and chromatin. At a morphological level, the organization and dynamics of these nuclear structures are suggested to play an active role in the activation and repression to gene expression and consequently to be required for healthy cell proliferation and maintenance [1]. For this reason, imaging/mapping nuclear structures within intact eukaryotic nuclei is pivotal to understand the effect of nuclear dynamic interactions on genome function. In last decades key innovations, such as fluorescence and confocal laser scanning microscopy (CLSM), made optical microscopy one of the most powerful tool to study the organization of nuclear compartment [2]. However, inside an intact cell nucleus, the size range of biological complexes goes below the conventional resolution limit of about 200 nm imposed by the diffraction-limited point-spread-funcion (PSF) of CLSM [3]. One of the strategies to study chromatin organization at the nanoscale is to use FRET, a process sensitive to nanometer distances but limited to the 10 nm range [4–6]. The recently developed super-resolution fluorescence microscopy (SRM) techniques provide a spatial resolution tunable down to molecular levels (1–200 nm). For this reason, SRM methods are well suited to study organization and dynamics of biological complexes at the nanoscale within intact nuclei. Since the early 1990s, several SRM methods were applied to the nuclear compartment, including distinct approaches based on structured illumination microscopy (SIM) [7–9], single-molecule localization microscopy (PALM, STORM) [10, 11] and stimulated emission depletion (STED) [12–14]. In last years, chromatin, nuclear lamina and the nuclear pore complex were visualized in different biological models by three dimension-SIM (3D-SIM) [15] and direct stochastic optical reconstruction microscopy (dSTORM) [16]. These works showed several features that escape detection by conventional microscopy, achieving a spatial resolution well below diffraction limit, e.g. under 20 nm for dSTORM. Moreover, super-resolved STED approach related to recent developed Expansion Microscopy technique (ExSTED) demonstrated an increase in resolution of up to 30-fold compared to conventional microscopy, providing a robust template for super-resolution microscopy of entire cells in the 10 nm range [17, 18]. The resolution of STED microscopy can reach the molecular size by increasing the intensity of the STED beam, but it is limited by other factors, such as the amount of laser power that can cause photodamage effects to the sample. For this reason, new strategies have been developed to reduce the peak power of the STED beam necessary to reach a given spatial resolution. An example is represented by time-gated Continuous-Wave STED microscopy (gCW-STED), which exploits the reduction of fluorophore lifetime due to the STED beam, reducing the depletion power more than 50% [19]. Theoretically, the spatial resolution of the gated STED microscope improves with the time-delay, but since a portion of photons from the PSF center is also discarded, the limiting factor becomes the signal-to-noise ratio (SNR). This can be made worse by the presence of uncorrelated background signal, such as that generated by direct excitation from the CW-STED beam [19–21].

In last years, our group introduced a novel approach to achieve the nanoscale resolution required to image nuclear structures: separation of photons by lifetime tuning (SPLIT) [22]. SPLIT can be applied to any STED image containing an additional temporal channel with encoded spatial information. For instance, in CW-STED, this additional temporal channel is the excited-state fluorescence lifetime [22–24]. In CW-STED, the lifetime of the fluorophores in the center of the point spread function (PSF) is longer than the lifetime of those located in the periphery of the PSF [19, 22]. To improve the spatial resolution of a CW-STED microscope, SPLIT extracts, at each pixel, the fraction of the signal corresponding to the longer fluorescence lifetime. To extract this fraction, SPLIT performs a phasor analysis of the time-resolved data, namely, the nanosecond fluorescence intensity decay at each pixel of the image is transformed from time to frequency domain and represented as a phasor. The phasor is used to isolate the fractional component of the intensity emitted from the center of the PSF (longer lifetime) from that emitted from its periphery (shorter lifetime). This fractional component contains only the signal emitted from a sub-diffraction spatial region (smaller than the PSF) and can be used to generate an image with improved spatial resolution. An advantage of lifetime-based SPLIT is the intrinsic removal of direct excitation from the STED beam from the final image [22]. On the other hand, the generation and observation of fluorescence lifetime gradients requires pulsed excitation and dedicated fast electronic hardware for lifetime detection in the nanosecond temporal scale, which are not available on every STED microscope.

Recently, we have overcome this limitation by applying the SPLIT algorithm to STED images obtained with modulated depletion power [25]. The results of this work clearly demonstrated that the 'spectroscopy' approach to super-resolution microscopy proposed by SPLIT is not limited to the analysis of fluorescence lifetimes but can have a more general application in STED microscopy. In this case, the additional channel for SPLIT was represented by the depletion power, a parameter that can be easily tuned on any STED microscope, without the need for dedicated excited-state lifetime detection hardware. In a straightforward implementation, we demonstrated that SPLIT could be applied to stacks of STED images acquired sequentially at increasing depletion power [25]. Application of SPLIT to the stacks resulted in improved super-resolution imaging of nuclear transcription and replication foci in fixed cells [25].

Optimal STED imaging of a given sample always relies on the proper tuning of several acquisition parameters, including the depletion and excitation powers, and the integration time. In particular, a major limitation to the total number of photons that can be collected during STED imaging is represented by the onset of photobleaching. For this reason, the acquisition of a stack of a number M of STED images, required for SPLIT, may present some practical limitations. For instance, in the specific implementation described in [25], a stack of $M = 8$ images was generated by linearly increasing the value of STED power P_{STED} from zero ($P_{\mathrm{STED}} = 0$) up to a maximum

value ($P_{STED} = P_{max}$), keeping a constant laser excitation power. Even if one has already optimized the STED imaging parameters for a given sample at the STED power P_{max}, these parameters must be carefully modified for the acquisition of a stack of n frames with STED power varying from 0 to P_{max}. In fact, in addition to the number of photons N required for the acquisition of the STED image at P_{STED}, one has to collect an extra number of photons $\sim (M-1) \times N$ for the acquisition of the other $M-1$ images of the stack, which is likely to results in more severe photobleaching.

For a given depletion power, the photobleaching rate is expected to increase at higher excitation powers and/or longer integration times. Thus, the level of the excitation power plays a critical role in optimizing the acquisition of the stack of STED images required for SPLIT.

Here, we explore which are the potential advantages of modulating also the excitation power during acquisition of a SPLIT stack of STED images at modulated depletion power. The main advantage of modulating the excitation power is that the number of photons collected can be tuned independently for each STED image of the stack. This has mainly two effects on the data. The first is that the susceptibility to photobleaching can be modulated by varying the number of photons acquired at the different STED powers. This aspect is important to reduce photobleaching and improve compatibility with live cell imaging. The second effect is that one may generate a SPLIT stack composed of single frames with very different signal-to-noise ratio (SNR). In this respect, we verify that, despite the variations of SNR, it is possible to generate a final SPLIT image with improved spatial resolution compared to the STED image of highest power. We apply this methodology to the imaging of nuclear structures, such as nuclear lamin and the nuclear pore complex (NPC), in fixed and live eukaryotic cells. In summary, our data demonstrate that the simultaneous modulation of STED and excitation power improves the versatility of the SPLIT-STED method for super-resolution imaging of nuclear structures.

2. Methods

2.1. The SPLIT-STED method

In this Section, we review the basis of the SPLIT method. We start from the most general formulation of the SPLIT method, and we end with its application in the context of STED microscopy imaging. In particular we use this general formulation to describe the two main SPLIT-STED implementations demonstrated so far. In the most general view, the SPLIT method bases on the ability to collect a fluorescence multi-dimensional 'image' $F(\mathbf{x},k)$, where $\mathbf{x} = (x,y,z)$ represents the conventional spatial dimension, and k an additional dimension able to encode extra spatial information about the specimen [26]. Given this multi-dimensional 'image', the SPLIT algorithm decodes such extra spatial information to obtain a final image $F_{SPLIT}(\mathbf{x})$, whose effective resolution is higher than any counterpart image obtained by integrating the multi-dimension image, i.e. $F_{sum}(\mathbf{x}) = \Sigma_k F(\mathbf{x},k)$, or selecting any value for the dimension k, i.e. $F(\mathbf{x}|k)$.

In a nutshell, the SPLIT method is composed by three main ingredients. The first ingredient consists in 'physically' introducing a sub-diffraction spatial signature in the fluorescence signal originating by each fluorophore located in the detection volume (or point spread function (PSF)) of a scanning microscope, i.e. each single-fluorophore (SF) must produce a 'different' fluorescent signal $f_{SF}(k,r)$ which depends by its distance r from the centre of the detection volume, $r = 0$. In particular, the term 'different' means that for any pair of values (r_1, r_2) the functions $f_{SF}(k,r_1)$ and $f_{SF}(k,r_2)$ must be linear independent. The second ingredients consists in using this spatial signature to separate the whole fluorescence signal collected in a specific position of the sample $F_{sum}(\mathbf{x})$, in two (or more) components, respectively the fluorescence generated by the fluorophores located in the central regions of the detection volume, $F_{in}(\mathbf{x}) = \Sigma_k F_{in}(\mathbf{x},k)$, and the fluorophores located in the periphery, $F_{out}(\mathbf{x}) = \Sigma_k F_{out}(\mathbf{x},k)$. Thanks to the linear independency described above, signal separation can be performed using the phasor representation and its linearity property, without the request of complex error-prone fitting methods. The third ingredient simply consists in the iteration of the signal separation for every pixel of the multi-dimensional 'image' $F(\mathbf{x},k)$. Indeed, the final SPLIT image with higher resolution will be obtained by using only the strength (or photons) of the signal from the central region, $F_{SPLIT}(\mathbf{x}) = F_{in}(\mathbf{x})$.

To describe in details the SPLIT method and the phasor-based signal separation we introduce two specific SPLIT-STED implementations, which use the process of stimulated emission to provide the first ingredient, namely to generate a set of linearly-independent function $f_{SF}(k,r)$. For sake of clarity, we assume that all fluorophores in the detection volume are located in two concentric rings with distance from the center r_{in} and $r_{out,}$ respectively. Clearly, in the real case fluorophores can be located in any positions of the detection volume, however, this 'discretization' does not introduce significant change in the results, but substantially reduces the complexity of the problem.

The first SPLIT-STED implementation [22] uses the temporal dimension of the excited-state fluorescence decay [19] as dimension to encode spatial information in the fluorescence signal (i.e. to generate a spatial signature in the fluorescence signal from a single-fluorophore). In a pulsed excitation, CW-STED microscopy experiment the fluorescence decay of a single-fluorophore as a function of the position r reads

$$f_{SF}(t,r) = I_{exc}(r) \exp\left(-t\left(k_{fl} + I_{STED}(r)\,\sigma_{STED}\right)\right), \quad (1)$$

with: $I_{exc}(r)$ and $I_{STED}(r)$ the co-aligned excitation and stimulated emission radial focal intensity distribution (the center of the Gaussian excitation profile is co-aligned with the 'zero-intensity' point of the doughnut-shaped stimulated emission profile), respectively; $k_{fl} = 1/\tau_{fl}$ the rate of spontaneous emission of the fluorophore (τ_{fl} the natural fluorescence lifetime of the fluorophore); σ_{STED} the stimulated emission cross-section of the fluorophore. In essence, since $I_{STED}(r)$ decreases in proximity of the center ($r = 0$), the closer the fluorophore is to the center of the detection volume the slower is its decay. This observation is the basis for improving the resolution of

STED microscopy by time-gating detection: by collecting the fluorescence signal after a fix temporal delay from the excitation events, highlights the fluorescence signal from the fluorophores close to the center, while discarding fluorescence from fluorophores in the periphery.

In the second SPLIT-STED implementation [25], the spatial information is encoded in the fluorescence signal by using the power of the STED beam ($k = P_{\mathrm{STED}}$). Here, the STED architecture can collect a sequence of STED images at different STED beam power values. In the gated CW-STED microscope, the fluorescence signal of a single-fluorophore as a function of the position r can be expressed as [19]:

$$f_{\mathrm{SF}}\left(P_{\mathrm{STED}},r\right) \cong I_{\mathrm{exc}}\left(r\right)\left(k_{\mathrm{fl}}/\left(k_{\mathrm{fl}}+P_{\mathrm{STED}}a\left(r\right)\sigma_{\mathrm{STED}}\right)\right) \times \exp\left(-T_g\left(k_{\mathrm{fl}}+P_{\mathrm{STED}}a\left(r\right)\sigma_{\mathrm{STED}}\right)\right), \quad (2)$$

with: $a(r)$ the function that relates P_{STED} to the STED intensity, $I_{\mathrm{STED}}(r) = P_{\mathrm{STED}}\ a(r)$; T_g the time gating value. Note that for large values of T_g, equation (2) can be approximated by an exponential decay function, as described in Sarmento *et al* [25].

Notably, for both SPLIT-STED implementations, the fluorescent signal f_{SF} is non-linear with respect to the stimulated emission intensity I_{STED}. Thanks to this non-linearity, two fluorophores located at two different radial distances r_{in} and r_{out} will show linear independent fluorescence signals $f_{\mathrm{SF}}(k,\ r_{\mathrm{in}})$ and $f_{\mathrm{SF}}(k,\ r_{\mathrm{out}})$. Which is exactly the first—and mandatory—ingredient of the SPLIT methods. In other words, the non-linearity introduced by the stimulated emission process, together with the doughnut-shaped STED beam intensity profile allows introducing a sub-diffraction spatial signature in the fluorescence signal.

Thanks to the linear independences describe above, for each pixel $\mathbf{x}$, the fluorescence signal $F(\mathbf{x},k)$ registered from the associated 'discrete' detection volume (i.e. fluorophores are located only in two concentring ring of radius r_{in} and r_{out}) can be written as:

$$F\left(\mathbf{x},k\right) = F_{\mathrm{in}}\left(\mathbf{x},k\right) + F_{\mathrm{out}}\left(\mathbf{x},k\right) = N_{\mathrm{in}}\left(\mathbf{x}\right)f_{\mathrm{SF}}\left(k,r_{\mathrm{in}}\right) + N_{\mathrm{out}}\left(\mathbf{x}\right)f_{\mathrm{SF}}\left(k,r_{\mathrm{out}}\right), \quad (3)$$

with: $N_{\mathrm{in}}(\mathbf{x}) = \Sigma_k\, F_{\mathrm{in}}(\mathbf{x},k)$ and $\mathrm{N}_{\mathrm{out}}(\mathbf{x}) = \Sigma_k\, F_{\mathrm{out}}(\mathbf{x},k)$ the total fluorescent photons, or more in general the strengths, for the inner and outer signal; $\langle - \rangle$ the operator denoting the function normalization. It is clear that if $\langle f_{\mathrm{SF}}\rangle(k,r_{\mathrm{in}})$ and $\langle f_{\mathrm{SF}}\rangle(k,r_{\mathrm{out}})$ are known, the separation between the inner and the outer photons $N_{\mathrm{in}}(\mathbf{x})$ and $N_{\mathrm{out}}(\mathbf{x})$ can be obtained by fitting the signal $F(\mathbf{x},k)$. A robust, fitting-free, and fast method to obtain the same 'photons' separation can be obtained by using the phasor representation $\mathbf{P}(\mathbf{x}) = (g(\mathbf{x}), s(\mathbf{x}))$ of the signal $F(\mathbf{x},k)$. In particular, we calculate the Fourier transform (FT) along the dimension k of $F(\mathbf{x},k)$ to obtain its phasor representation. Thanks to the linear decomposition of $F(\mathbf{x},k)$, the phasor $\mathbf{P}(\mathbf{x})$ will be the vectorial superposition of the individual phasors $\mathbf{P}_{\mathrm{in}} = (g_{\mathrm{in}},s_{\mathrm{in}})$ and $\mathbf{P}_{\mathrm{out}} = (g_{\mathrm{out}},s_{\mathrm{out}})$ associated to $\langle f_{\mathrm{SF}}\rangle(k,r_{\mathrm{in}})$ and $\langle f_{\mathrm{SF}}\rangle(k,r_{\mathrm{out}})$ (figure 1(A))

$$\mathbf{P}\left(\mathbf{x}\right) = \left(N_{\mathrm{in}}\left(\mathbf{x}\right)/N\left(\mathbf{x}\right)\right)\mathbf{P}_{\mathrm{in}} + \left(N_{\mathrm{out}}\left(\mathbf{x}\right)/N\left(\mathbf{x}\right)\right)\mathbf{P}_{\mathrm{out}} = w_{\mathrm{in}}\left(\mathbf{x}\right)\mathbf{P}_{\mathrm{in}} + w_{\mathrm{out}}\left(\mathbf{x}\right)\mathbf{P}_{\mathrm{out}}. \quad (4)$$

Thus, for every pixel, and for a given pair of $\mathbf{P}_{\mathrm{in}}$ and $\mathbf{P}_{\mathrm{out}}$ (the same for each pixel and previously obtained by choosing appropriate value of r_{in} and r_{out}) it is possible to obtain the value of the fractions $w_{\mathrm{in}}(\mathbf{x})$ and $w_{\mathrm{out}}(\mathbf{x})$ by a matrix inversion

$$\begin{pmatrix} w_{\mathrm{in}}\left(\mathbf{x}\right) \\ w_{\mathrm{out}}\left(\mathbf{x}\right) \end{pmatrix} = \begin{pmatrix} g_{\mathrm{in}} & g_{\mathrm{out}} \\ s_{\mathrm{in}} & s_{\mathrm{out}} \end{pmatrix}^{-1} \begin{pmatrix} g\left(\mathbf{x}\right) \\ s\left(\mathbf{x}\right) \end{pmatrix}. \quad (5)$$

If it is present a fraction of the signal which is uncorrelated along dimension k, this fraction can be evaluated as $w_{\mathrm{uncorr}}(\mathbf{x}) = 1 - w_{\mathrm{in}}(\mathbf{x}) - w_{\mathrm{out}}(\mathbf{x})$. For instance, in the lifetime-based CW-STED implementation, the fraction w_{uncorr} can include background signal arising from unwanted, direct excitation of the fluorophores by the STED beam [23]. Otherwise, we can set $w_{\mathrm{in}}(\mathbf{x}) + w_{\mathrm{out}}(\mathbf{x}) = 1$, and equation (4) can be rewritten as:

$$\mathbf{P}\left(\mathbf{x}\right) = w_{\mathrm{in}}\left(\mathbf{x}\right)\mathbf{P}_{\mathrm{in}} + \left(1 - w_{\mathrm{in}}\left(\mathbf{x}\right)\right)\mathbf{P}_{\mathrm{out}}. \quad (6)$$

From which:

$$w_{\mathrm{in}}\left(\mathbf{x}\right) = \left|\mathbf{P}\left(\mathbf{x}\right) - \mathbf{P}_{\mathrm{out}}\right| / \left|\mathbf{P}_{\mathrm{in}} - \mathbf{P}_{\mathrm{out}}\right|. \quad (7)$$

Finally, the high-resolution SPLIT-STED image $F_{\mathrm{SPLIT}}(\mathbf{x})$ is given by

$$F_{\mathrm{SPLIT}}\left(\mathbf{x}\right) = \sum\nolimits_k F_{\mathrm{in}}\left(\mathbf{x},k\right) = w_{\mathrm{in}}\left(\mathbf{x}\right)\sum\nolimits_k F\left(\mathbf{x},k\right) = w_{\mathrm{in}}\left(\mathbf{x}\right)N\left(\mathbf{x}\right). \quad (8)$$

2.2. SPLIT-STED with tunable depletion and excitation power

In this section we introduce new strategies to further enhance the effective resolution of the SPLIT-STED implementation based on the tunability of the STED/depletion beam power. These strategies allow to obtain images whose effective resolution would be achieved by conventional STED imaging (or by any other SPLIT-STED imaging) only by using higher intensities of the STED beam, thus higher potential photodamage.

Equation (8) shows that the improvement of spatial resolution of the SPLIT image is provided by the fraction $w_{\mathrm{in}}(\mathbf{x})$ extracted by the phasor analysis of the multi-dimensional image $F(\mathbf{x},k)$ along the additional channel k. Equation (8) also shows that the signal-to-noise ratio (SNR) of the SPLIT image will be affected by any additional noise introduced by $w_{\mathrm{in}}(\mathbf{x})$. In fact, $w_{\mathrm{in}}(\mathbf{x})$ is calculated by decomposition of the phasor $\mathbf{P}(\mathbf{x})$ which, in turn, is affected by an experimental error dependent on the total number of photons detected at a given pixel.

In the SPLIT-STED implementation based on tunable depletion power, described in Sarmento *et al* [25], $F(\mathbf{x},k)$ represents a stack of STED images acquired at increasing STED power and constant excitation power (figure 1(B)). In this implementation, the fluorescence intensity of a fluorophore located in the center ($r = 0$) of the detection volume (or PSF), $f_{\mathrm{SF}}(k,r = 0)$, is constant as a function of k, whereas that of a fluorophore located in its periphery, $f_{\mathrm{SF}}(k,r > 0)$, decays as a

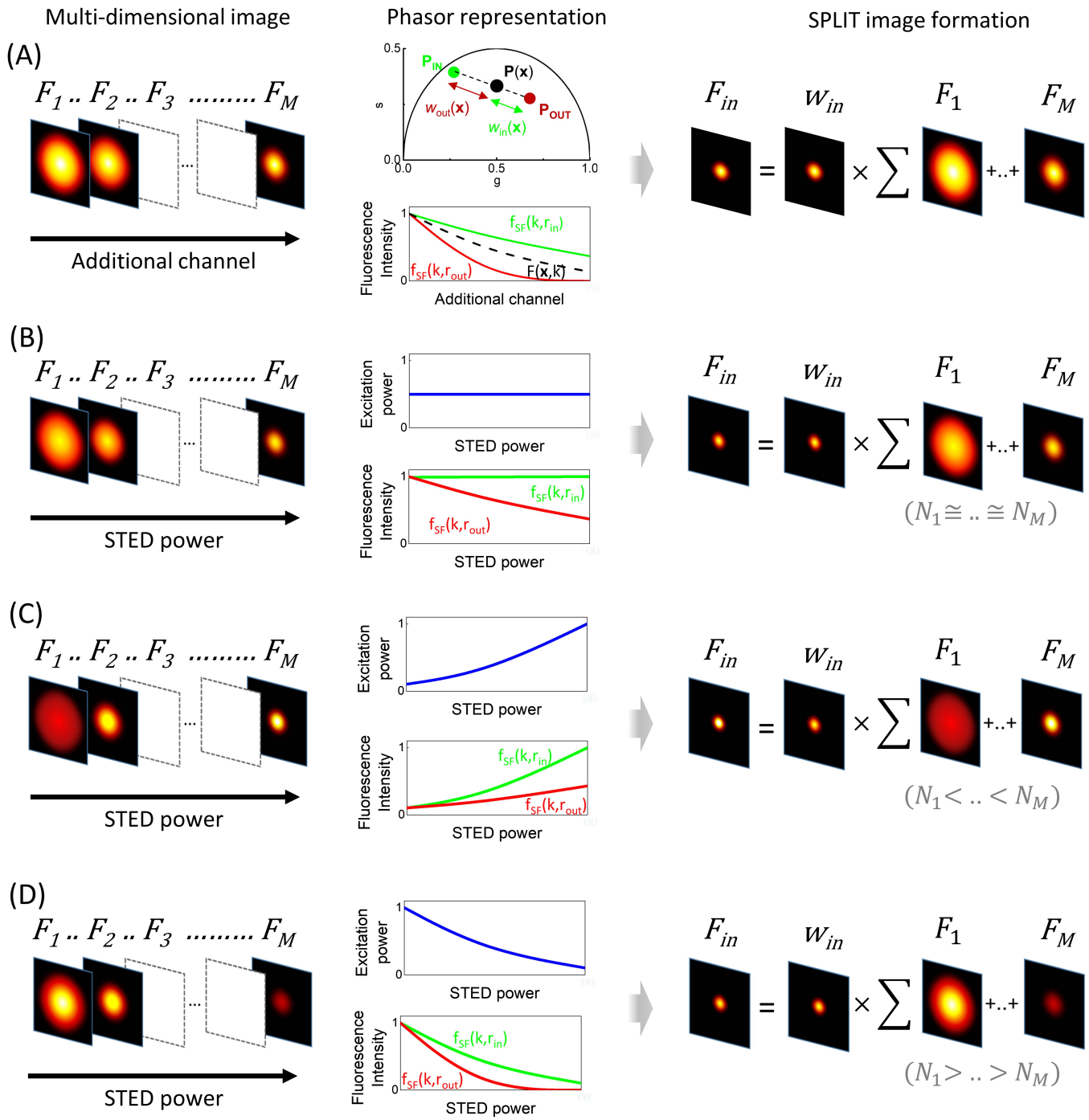

Figure 1. Schematic principle of different SPLIT-STED configurations. The multi-dimensional image $F_{1\ldots M}$ contains an extra spatial information encoded in an additional channel. In (A), the extra information is represented by fluorescence lifetime gradient, generated by the depletion effect of a CW-STED within the PSF. The phasor analysis decodes the fluorescence information $P(x)$ into two different fluorescence population P_{IN} and P_{OUT}. The $f_{\mathrm{SF}}(k,r_{\mathrm{in}})$ represents the fluorescence signal of the phasor component P_{IN} (center of the PSF), whereas the $f_{\mathrm{SF}}(k,r_{\mathrm{out}})$ the fluorescence signal of the phasor component P_{OUT} (periphery of the PSF). In (B)–(D), the extra information is provided by increasing the STED power from F_1 to F_M. The intensity curves $f_{\mathrm{SF}}(k,r_{\mathrm{in}})$ and $f_{\mathrm{SF}}(k,r_{\mathrm{out}})$ show the fluorescence depletion dynamics of a single fluorophore arising from the center (in) and the periphery (out) of the PSF, along the stack. The fluorescence signal depends on the excitation pattern (blue line). In (B), the excitation power is kept constant, whereas in (C), (D) is exponentially modulated. In all the configurations (A)–(D), the SPLIT image F_{in} is generated by the SPLIT algorithm by the fraction w_{in}, obtained by the phasor analysis, multiplied for the integrated image $F_{\mathrm{sum}} = \Sigma\, F_1 + \ldots + F_M$. The distribution of photons N along the STED stack depends on the excitation pattern.

result of the increasing action of the STED beam (figure 1(B)). Since the excitation power is kept constant, each STED image of the stack is collected with roughly a constant peak signal-to-noise ratio, i.e. for each detection volumes the number of photons collected from the central region ($r = 0$) is constant with respect to k, $N_1 \sim N_2 \sim \ldots \sim N_k \sim \ldots \sim N_M$ (figure 1(B)), with M the number of different values for the STED beam power. The integrated image $F_{\text{sum}}(\mathbf{x})$, used for formation of the SPLIT image, has a spatial resolution intermediate between the STED image acquired at minimum STED power, $F_{k=1}(\mathbf{x})$, and the STED image acquired at maximum STED power, $F_{k=M}(\mathbf{x})$.

Here, we introduce a modified SPLIT-STED implementation in which we tune also the excitation power during the acquisition multi-dimension STED image (figures 1(C) and (D)). In this implementation, the maximum number of photons N_k collected for each STED image of the stack can be tuned independently. As a result, one can generate different SPLIT data acquisition scenarios. For instance, one can increase the excitation power concomitantly with the depletion power, in order to get more photons at the higher STED powers and thus get a higher SNR in the frames containing higher spatial frequencies (figure 1(C)). In this case, the integrated image $F_{\text{sum}}(\mathbf{x})$ used for formation of the SPLIT image has a spatial resolution closer to that of the STED image of maximum resolution, $F_{k=M}(\mathbf{x})$. This improvement of resolution comes at the expense of an increased level of photodamage. Conversely, one can decrease the excitation power in opposition to the depletion power, to get less photons at the higher STED powers and thus reduce the potentially detrimental impact of simultaneous high excitation and STED powers (figure 1(D)). In this second case, we expect a significant reduction of photodamage. However, this reduction of photodamage comes at the expense of a lower resolution. In fact, the integrated image $F_{\text{sum}}(\mathbf{x})$ used for SPLIT has a spatial resolution closer to the image of the stack with minimum resolution $F_{k=1}(\mathbf{x})$.

2.3. Cells culture and sample preparation

HOS, HEK and HeLa cells were cultured in Dulbecco's modified Eagle's medium (DMEM) (Sigma-Aldrich) supplemented with 10% FBS, 2 mm L-glutamine and 1% penicillin/streptomycin in a humidified incubator at 37 °C with 5% CO_2. PC3 cells were cultured in Ham's F12K (Thermo Fisher Scientific) medium containing 7% FBS, 2 mm L-glutamine and 1% penicillin/streptomycin. Cells were grown in humidified incubator at 37 °C with 5% CO_2. For nuclear pore immunolabeling, immunofluorescence was carried out as described previously [18]. Human osteosarcoma (HOS) cells were plated at 70% confluency on 18 mm coverglass and grown overnight. The cells are pre-extracted with 2.4% PFA and 0.3% Triton-X100 in PBS for 3 min. After fixation with 2.4% PFA for 30 min, the cells are blocked for 1 h with 5% BSA. Then, the cells are incubated overnight at 4 °C with primary antibody anti-Nup153 (ab84872; AbCam) in BSA 5%. After washing several times in PBS, the cells are incubated with the secondary antibody Alexa488 (A28175; Thermofisher Scientific) at room temperature for 1 h. Human embryonic kidney (HEK) cells were fixed with ice-cold methanol for 10 min at −20 °C. After incubation in BSA, the cells were incubated with primary antibody anti-lamin B2 (33–2100; Thermofisher Scientific) overnight at 4 °C. After several washes in PBS, the cells were incubated with the secondary antibody Alexa Fluor 488 (A28175; Thermofisher Scientific) at room temperature for 1 h.

For live cell imaging, HeLa cells cells were plated on Ibidi μ-slide 8-well chambered coverslips and let grow overnight at 60%–80% confluence. After 24 h, cells were transiently transfected with SNAP-tag Lamin A (Plasmid #58193; Addgene), according to QIAGEN Effectene protocol. For SNAP-tag labeling, we used 5 μm cell-permeable SNAP-cell 505-star dye (New England Biolabs Inc.) in complete medium with 0.5% BSA, and left incubating for 30 min at 37 °C. After cells were washed three times with the culture medium (Cellular Labeling protocol S9103; New England Biolabs Inc.).

2.4. Experiments

All imaging experiments were performed on a Leica TCS SP5 gated-CW-STED microscope, using a HCX PL APO × 100 100/1.40/0.70 oil immersion objective lens (Leica Microsystems, Mannheim, Germany). Emission depletion was accomplished with a 592 nm STED laser. Excitation was provided by a white laser at the desired wavelength for each sample. Alexa 488 and SNAP-cell 505-star were excited at 488 nm and the fluorescence emission detected at 500–560 nm. Time gating was set 1.5–10.0 ns for all the images. The frame size was set to 512 × 512 pixels (Lamin A, Nup153) and 1024 × 1024 pixels (Lamin B). Stacks of $M = 3$ STED images with different STED power were obtained using the line sequential acquisition mode (1400 Hz). The STED power in the 3 images was set to 0, $P_{\text{max}}/2$ (12.5 mW), P_{max} (25 mW), respectively. The excitation level in the 3 frames was set to a constant value or tuned according to an exponential pattern:

$$P_{\text{exc}}(k) = P_{\text{exc}}(1)\, e^{\frac{k-1}{\tau_{\text{exc}}}} \tag{9}$$

where $P_{\text{exc}}(1)$ is the excitation power at frame number 1, and the constant τ_{exc} was set to $\tau_{\text{exc}} = 1$ and $\tau_{\text{exc}} = -1$, respectively. Both STED and excitation powers were measured after the objective, at the sample plane.

2.5. Simulation and data analysis

Simulated STED image stacks were generated using MATLAB. The object consisted of point-like emitters distributed randomly. To create the image stacks, the objects were convolved with the following PSF of a STED microscope [25, 27]:

$$i(r,k) = N(k)\, \mathrm{e}^{-\frac{2r^2}{w^2}}\, \mathrm{e}^{-\varsigma(k)\frac{r^2}{w^2}} \tag{10}$$

where $N(k)$ is the maximum number of counts per particle, $r = (x^2 + y^2)^{1/2}$, w is the width of the confocal PSF, $\varsigma(k)$ is the STED saturation factor at radial position $r = w$. Each stack consisted of a number $M = 3$ of 128 × 128 frames with a pixel

size of 20 nm. The STED saturation factor was varied along the stack as $\varsigma(1) = 0, \varsigma(2) = \varsigma_{max}/2, \varsigma(3) = \varsigma_{max}$ with $\varsigma_{max} = 10$. The waist of the confocal PSF was set to $w = 320$ nm.

To simulate different patterns of the excitation tuning, the prefactor $N(k)$ in equation (10) was set to an exponential function:

$$N(k) = N(1)\, e^{\frac{k-1}{\tau_{exc}}} \tag{11}$$

where $N(1)$ is the maximum number of counts per particle in the first frame and the constant τ_{exc} can take both positive and negative values. Poisson noise was introduced to each pixel at a level based on the pixel value using the MATLAB function 'imnoise'.

For each stack, the SPLIT analysis was performed in Matlab using a previously described algorithm [25], adapted to take into account the tuning of the excitation intensity. Briefly, For a given image stack $F(\mathbf{x},k)$, the phasor components $g(\mathbf{x})$ and $s(\mathbf{x})$ were calculated performing a FT of $F(\mathbf{x},k)$ along k. Then the phasor components g_{exc} and s_{exc} corresponding to the known excitation pattern (equation (11)) were subtracted from $g(\mathbf{x})$ and $s(\mathbf{x})$. In this way, the experimental phasor is located close to the origin, independently of the specific excitation pattern used. Then the fraction $w_{in}(\mathbf{x})$ was calculated by splitting the signal into two components, using equation (7), where the positions of the phasors $\mathbf{P}_{in}$ and $\mathbf{P}_{out}$ were determined following the procedure described by Sarmento *et al* to visualize the spatial information encoded by the phasor, we calculated the parameter $m(\mathbf{x}) = (g(\boldsymbol{x})^2 + s(\boldsymbol{x})^2)^{1/2}$, representing the modulus of the phasor.

Fourier ring correlation (FRC) analysis was performed in Matlab as reported previously [28]. Image spatial autocorrelation functions (ACF) were calculated in Matlab using the algorithm described in [29]. The ACFs were fitted to a Gaussian model to extract the average width of the effective PSF expressed as full width at half maximum (FWHM).

3. Results

3.1. SPLIT-STED imaging of simulated data

To verify that the STED stacks obtained with the new implementation could be used to produce SPLIT images, we simulated images of random distributions of point-like particles. The simulated stacks consisted of $M = 3$ STED images generated to simulate increasing STED power throughout the stack, and different patterns of the excitation intensity. We chose $M = 3$ to further simplify the acquisition settings. The modulation of the excitation intensity along the stack depends only the constant τ_{exc}, which can take both positive and negative values. If $\tau_{exc} > 0$, the excitation has an exponential growth, if $\tau_{exc} < 0$ the excitation has an exponential decay (figure 2).

In figure 2 we compare simulated data obtained with excitation patterns corresponding to $\tau_{exc} = 1$ (figure 2(A)), $\tau_{exc} = \infty$ (i.e. constant excitation level, figure 2(B)) and $\tau_{exc} = -1$ (figure 2(C)). The data have been simulated with the same maximum total number of counts per particle, $N(1) + N(2) + N(3) = 20$. For each condition, we show the first and last frame of the stack, the phasor plot and the SPLIT image (figure 2). For a visual comparison, the phasor plots corresponding to $\tau_{exc} = 1$ and $\tau_{exc} = -1$ have been translated towards the origin by subtracting the FT of the known excitation pattern (see Methods). In all three cases, the information encoded in the variations of STED power can be used to produce a SPLIT image with higher spatial resolution than the STED images, as quantified by FRC [28] or spatial autocorrelation function (ACF) (figures 2(A)–(C)). The difference between the resolution enhancements retrieved by the FRC and ACF analysis is likely due to the higher noise sensitivity of the FRC method. Thus, the SPLIT approach can be applied to STED stacks obtained by simultaneous modulation of STED and excitation power, despite the significant variations of SNR along the stack.

The integrated image used for formation of the SPLIT image in equation (8) can also be obtained by a partial sum of the frames of the stack. For instance, one may want to include in the integrated image only the STED frames with higher spatial resolution. We tested by FRC if there was any advantage in using only the last frame F_3 or the sum of the last two frames, F_{2-3} (figure S1 (stacks.iop.org/JPhysD/53/234003/mmedia)). The results of this analysis show no significant difference between the SPLIT images calculated using the total or a partial sum of the frames of the stack. This indicates that, in the simulations, the potential advantage of excluding the frames with poorer spatial resolution is counterbalanced by the reduction in the number of photons used for the final image.

3.2. SPLIT-STED imaging with improved SNR in fixed cells

To evaluate the extent of photobleaching in the different SPLIT-STED configurations, corresponding to $\tau_{exc} = 1$, $\tau_{exc} = \infty$ and $\tau_{exc} = -1$, we performed a time-lapse acquisition. In particular, we measured the photobleaching kinetics occurring under the depletion power by 592 nm STED beam in fixed HeLa cells. In particular, we visualized the α-tubulin labeled with Alexa Fluor 488 (see Methods). As expected, all the excitation patterns showed a general decrease of the fluorescence signal, but the configuration with negative constant τ_{exc} produced less photobleaching on the specimen compared with the configuration with $\tau_{exc} = 1$ and $\tau_{exc} = \infty$, probably thanks to the lower excitation of the sample in the time window in which the power of STED is at maximum (F_3 image). This suggests that this SPLIT-STED configuration could be useful to minimize the effects of photobleaching and phototoxicity in live samples (figure S2).

We tested the first SPLIT-STED configuration, namely excitation modulation with positive constant τ_{exc}, for the imaging of fixed cells. In particular, we visualized nuclear lamin-B and the nuclear pore complex (NPC) protein Nup153, labeled with Alexa Fluor 488 (see Methods). In this configuration, the last frame (F_3) of the stacks, should contain the best resolved structures, due to the maximum depletion power by 592 nm STED beam, and also the highest SNR, due to the maximum level of the excitation power (figures 3(A), (G) and (M)).

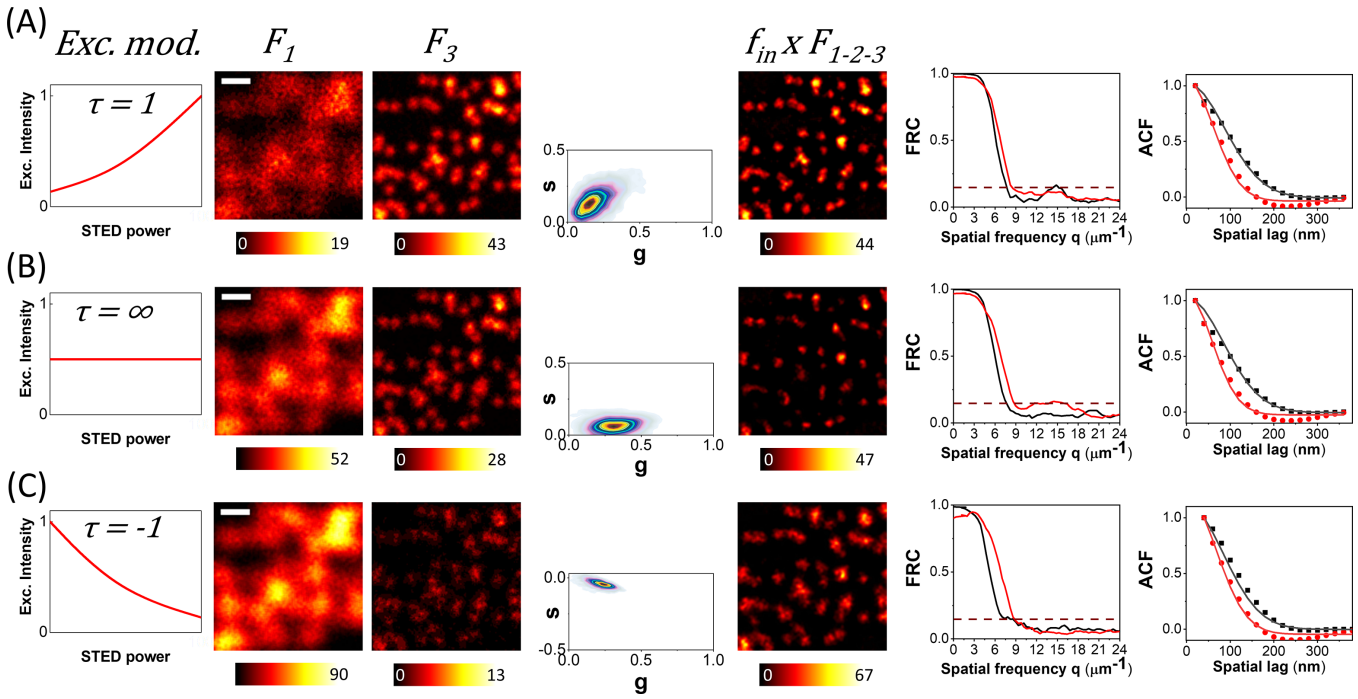

Figure 2. Excitation patterns and phasor analysis in SPLIT-STED. Simulations of nuclear spots under different conditions of acquisition. (A)–(C) were simulated with the same STED saturation factor $\varsigma_{max} = 10$. The SNR varies depending on the synchronized effect of the STED power and the excitation power modulation (red excitation curve). The simulations were implemented with three different excitation patterns: $\tau_{exc} = 1$ (A), $\tau_{exc} = \infty$ (B) and $\tau_{exc} = -1$ (C). For each simulation (from left to right): the average variation of fluorescence intensity in the first and last image of the stack (F_1 and F_3), the corresponding phasor plot, the final SPLIT image obtained by multiplying the fraction F_{in} with the sum of $F_1 + F_2 + F_3$, the FRC curves corresponding to the effective resolution of the STED image F_3 (black) and the SPLIT images (colored) and the spatial correlation functions of the STED image F_3 (black squares) and the SPLIT image (red circles). The FRC analysis showed the following resolution values: for $\tau_{exc} = 1$, 128 nm (STED) and 116 nm (SPLIT); for $\tau_{exc} = \infty$, 128 nm (STED) and 111 nm (SPLIT); for $\tau_{exc} = -1$, 135 nm (STED) and 128 nm (SPLIT). The autocorrelation function measured the width of the PSF, expressed as FWHM: for $\tau_{exc} = 1$, $FWHM_{STED} = 144$ nm and $FWHM_{SPLIT} = 104$ nm; for $\tau_{exc} = \infty$, $FWHM_{STED} = 142$ nm and $FWHM_{SPLIT} = 97$ nm; and for $\tau_{exc} = -1$, $FWHM_{STED} = 139$ nm and $FWHM_{SPLIT} = 113$ nm. Scale bar: 1 μm.

For each acquisition, we show the phasor plot and the map of the parameter m, which describes the variation along the main axis of symmetry of the phasor (see Methods). Both the phasor plot and the $m(\mathbf{x})$ map reveal the encoded spatial information used to produce the SPLIT image. To estimate the improvement of spatial resolution, we show line profiles and the FRC analysis.

By fitting the line profile with single- and multi-peak Gaussian function, we estimate the apparent size of these biological structures. The line profile of the nuclear pore complex (NPC) image shows $FWHM_{F3} \sim 127$ nm and $FWHM_{Fin} \sim 87$ nm. Nuclear B-lamin was analyzed in median and apical focal planes showing its structure from different point of view. We estimate the FWHM at the median plane to be ~192 nm in F_3 and ~61 nm in F_{in}, whereas, at the apical plane, is ~88 nm and ~72 nm in F_3 and ~64 nm and ~31 nm in F_{in}. The improvement of spatial resolution is also confirmed by FRC analysis performed on the same data (figures 3(F), (L) and (R)).

These values represent a strong improvement in resolution of tens of nanometers, reinforcing the usefulness of the modulation of excitation for the SPLIT algorithm. However, this configuration has significant higher level of photobleaching compared to the configurations with $\tau_{exc} = \infty$ and $\tau_{exc} = -1$, due to the detrimental impact of simultaneous high excitation and STED powers (figure S2).

3.3. SPLIT-STED imaging with reduced photobleaching in live cells

We then tested a second SPLIT-STED configuration, in which the excitation was modulated exponentially with negative constant τ_{exc}. We tested this configuration on live HeLa cells transfected with SNAP-tag Lamin A and labeled with the SNAP-cell 505-star dye. Here we acquired the images of the stacks modulating the excitation laser with an exponential decay from the frame F_1 to F_3 (figure 4(A)). As shown in figure 4(A), the confocal image F_1 ($I_{exc} = \max$, $I_{STED} = 0$) contained the highest fluorescence intensity signal, in opposite to F_3 image ($I_{exc} = \min$, $I_{STED} = \max$), where the intensity signal is very low, due to the synchronized effect of a weak excitation power with maximum depletion power. Also in this case, we were able to produce a SPLIT image F_{in} with better spatial resolution than the STED image (figures 4(C) and (D)). However, as we can observe from the F_3 image and, consequently, from its line profile, the signal-to-noise ratio was too low to determine a value of FWHM. Therefore, we compare the SPLIT image ($FWHM_{Fin} \sim 140$ nm) with the integrated image $F_{1\text{–}3}$ ($FWHM_{Fsum} \sim 305$ nm).

This configuration ($\tau_{exc} = -1$) produced less photobleaching on the specimen compared with the configuration with $\tau_{exc} = 1$, probably thanks to the lower excitation of the sample

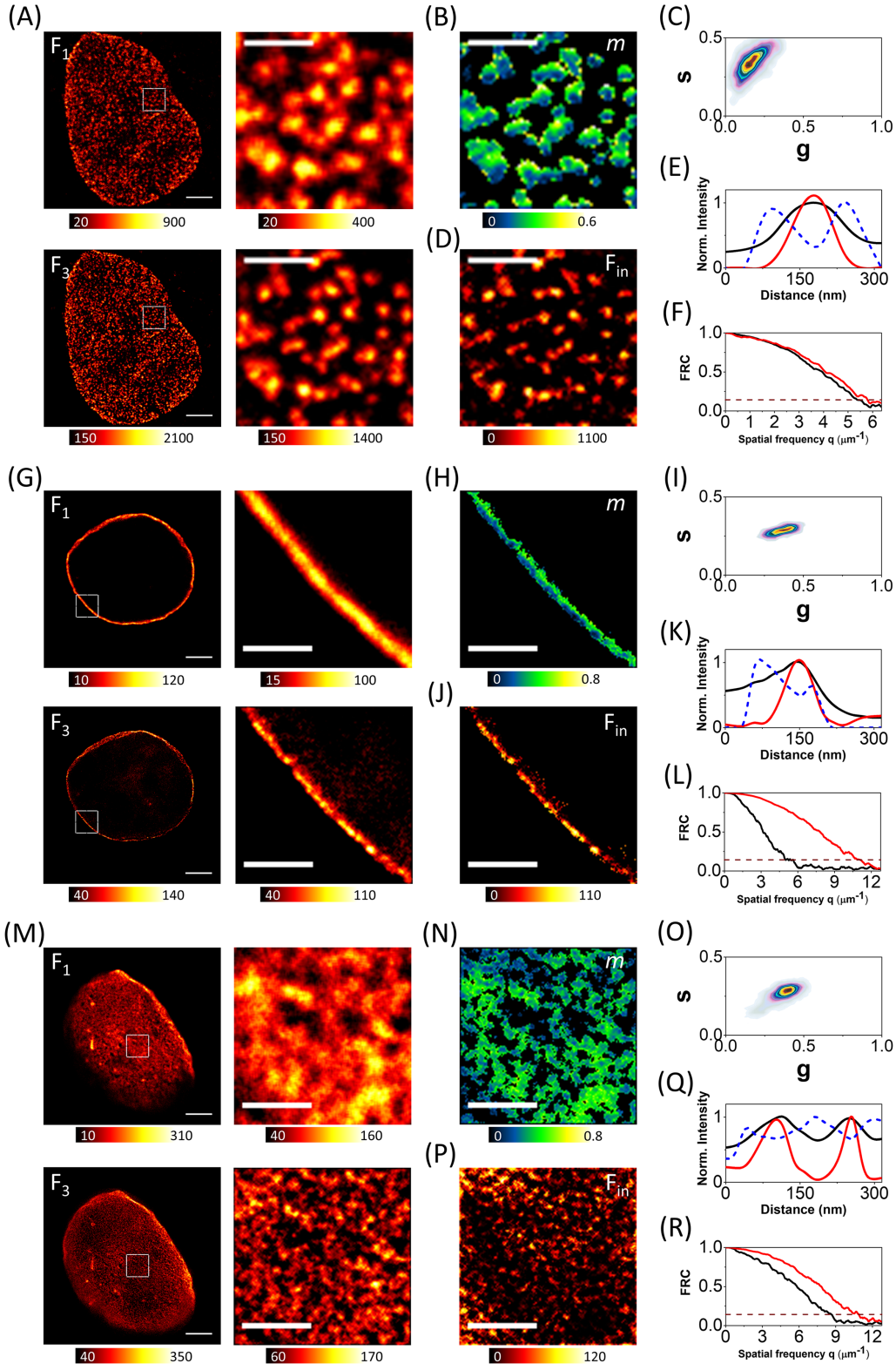

Figure 3. SPLIT-STED of nuclear structures within intact nuclei of fixed cells. (A), (G), (M) Acquired stack images of Nup153 (A), median (G) and apical (M) Lamin-B, from the confocal (F_1) to maximum STED power (F_3) ($P_{max} = 25$ mW), with exponential increase of excitation power ($\tau_{exc} = 1$). Scale bar: 3 μm (scale bar ROI: 1 μm). (B), (H), (N) Image of the parameter m. Color scale: m (0–0.6/0.8). (C), (I), (O) Corresponding phasor plots obtained from the data. Scale bar: 1 μm. (D), (J), (P) SPLIT image F_{in} obtained by application of SPLIT to F_3. Scale bar: 1 μm. (E), (K), (Q) Line profiles show the improvement of spatial resolution of nuclear structures from F_3 (black line) to F_{in} (red line), and the relation with the information encoded in the $m(\mathbf{x})$ image (dash blue line). (F), (L), (R) FRC analysis confirms the corresponding effective resolution of the STED image (black curve) and the SPLIT image (red curve). The FRC curves showed the following resolution values: for Nup153, 184 nm (F_3) and 172 nm (F_{in}); for median Lamin-B, 199 nm (F_3) and 90 nm (F_{in}); for apical Lamin-B, 115 nm (F_3) and 91 nm (F_{in}).

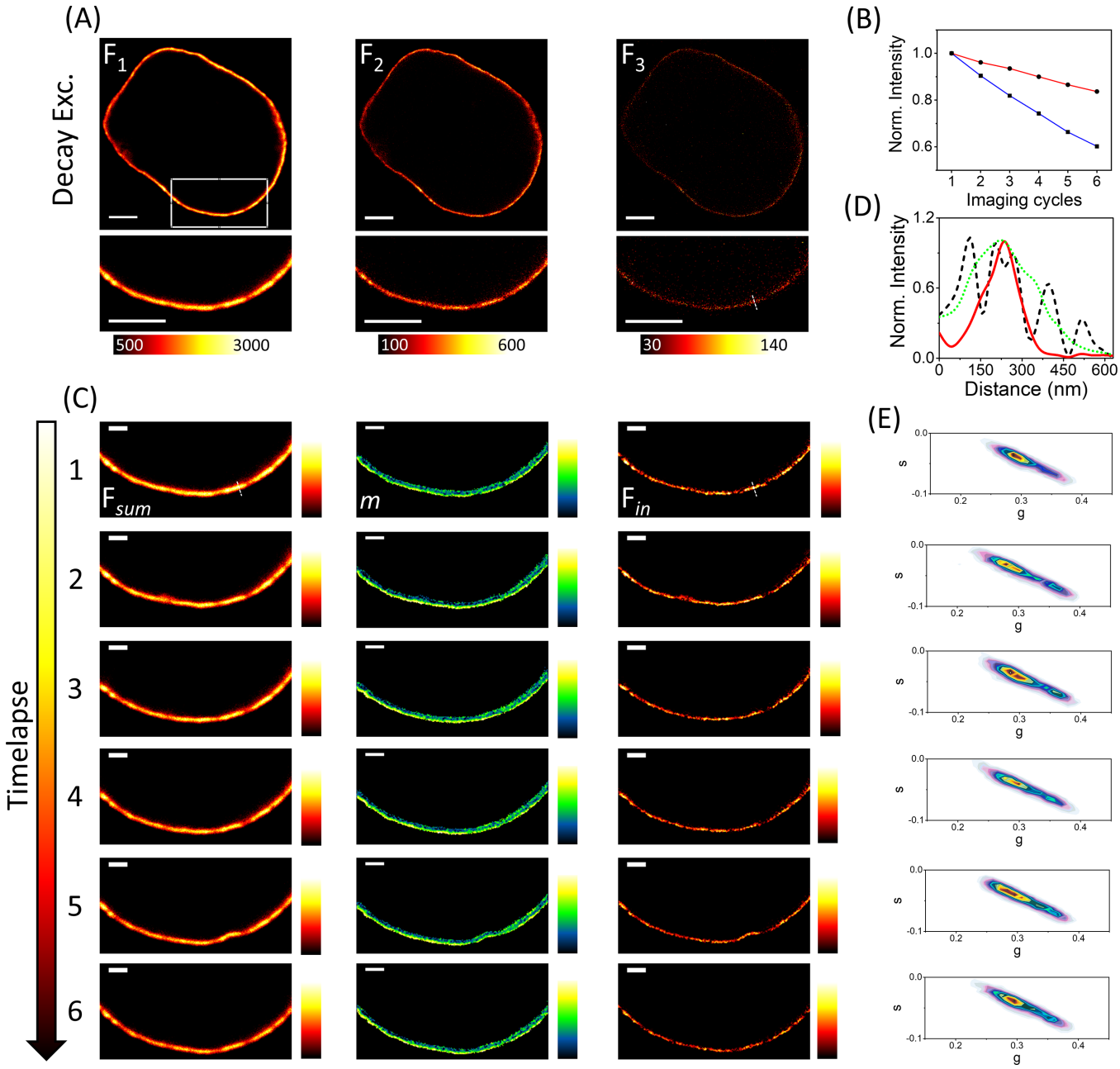

Figure 4. SPLIT-STED of nuclear Lamin-A in intact nuclei of live cells. (A) SPLIT-STED stack images of Lamin-A, from the confocal (F_1) to maximum STED power (F_3) ($P_{max} = 25$ mW), with exponential decay of excitation power ($\tau_{exc} = -1$). Scale bar: 3 μm. (B) Comparison between the photobleaching effect by using the $\tau_{exc} = -1$ (red intensity curve) and $\tau_{exc} = 1$ (blue intensity curve) excitation patterns, during a timelapse SPLIT-STED acquisition. For each imaging cycle (1–6) of the timelapse: (C) (from left to right) the integrated image $F_{sum} = F_1 + F_2 + F_3$, the image of the parameter m and the SPLIT image F_{in} obtained by application of SPLIT to F_{sum}, and (E) the corresponding phasor plots. Scale bar: 1 μm. (D) Line profiles show the effective spatial resolution of Lamin-A in F_{sum} image (dash green line), F_{in} image (red line) and F_3 image (dash black line).

in the time window in which the power of STED is at maximum (F_3 image). This suggests that this SPLIT-STED configuration could be useful to minimize the effects of photobleaching and phototoxicity in live samples (figures 4(B) and S3).

A time-lapse SPLIT-STED acquisition is reported in figures 4(b) and (C). Thanks to the reduced level of photobleaching, the number of photons collected per time-frame remains high enough to perform the SPLIT analysis, as demonstrated also by the $m(\mathbf{x})$ map and the phasor plot (figures 4(C) and (E)).

4. Discussion

The SPLIT approach is a simple and efficient way to improve the spatial resolution of a fluorescence multi-dimensional image $F(\mathbf{x},k)$, provided that the additional dimension k

encodes extra spatial information about the specimen. To decode extra spatial information, SPLIT performs a phasor analysis of the fluorescence signal along dimension k in a pixel-by-pixel manner. One of the key ingredients is the presence of non-linearity in the sub-diffraction spatial signatures $f_{SF}(k,r)$ that characterize the center and periphery of the PSF. More specifically, the functions $f_{SF}(k,r_1)$ and $f_{SF}(k,r_2)$ must be linearly independent, for any pair of values (r_1, r_2). In this work, and more in general in any SPLIT-STED approach, this non-linearity is introduced by using the non-linearity of the stimulated emission effect. Indeed, for $I_{STED}(r) = 0$, i.e. for the confocal case, the possibility of having linear independent fluorescence signals $f_{SF}(k,r)$ for two fluorophores located at different radial position vanishes. In the confocal time-resolved implementation, this impossibility is the direct consequence of the independence of the excited-state lifetime with the excitation intensity, i.e. the Gaussian excitation beam alone cannot introduce a spatial signature in the fluorophore lifetime (excited-state fluorescence decay). In the case of confocal tunable excitation power, this impossibility is due to the linear dependence between fluorescence signal and excitation intensity. However, the linear dependence between fluorescence and excitation intensity is broken in the case of fluorescence saturation effects, $I_{exc}(0)\sigma_{exc} \gg k_{fl}$, and spatial information can be encoded in a non-STED (conventional confocal) approach [30]. Thus, a new class of SPLIT implementation could be derived also for confocal microscopy, when intensity saturation effects are taken into account.

In this work, we have exploited the associated advantage tuning both the STED and excitation power, to improve the versatility of the SPLIT-STED approach. The tuning of the depletion power is used to produce STED images at different resolution and to generate the non-linearity required by the SPLIT method. The tuning of the excitation power is used to modulate the number of photons collected for each STED image. We have shown that the SPLIT-STED method produces an improvement of spatial resolution for very different tuning patterns of the excitation intensity. An interesting aspect emerging from our study is that the extent of photobleaching can be modulated by the excitation pattern, as it depends on the simultaneous impact of high STED and excitation powers. Thus, the tuning of the excitation power improves applicability of the method to live cell imaging, potentially minimizing the photobleaching of the fluorophores and the phototoxicity on the biological samples during a SPLIT-STED acquisition.

Acknowledgments

L L was supported by Associazione Italiana per la Ricerca sul Cancro (AIRC) under MFAG 2018—ID. 21931 project.

ORCID iDs

Simone Pelicci https://orcid.org/0000-0003-3539-8613
Giorgio Tortarolo https://orcid.org/0000-0002-1182-2478
Giuseppe Vicidomini https://orcid.org/0000-0002-3085-730X
Alberto Diaspro https://orcid.org/0000-0002-4916-5928
Luca Lanzanò https://orcid.org/0000-0001-6539-394X

References

[1] Soutoglou E and Misteli T 2007 Mobility and immobility of chromatin in transcription and genome stability *Curr. Opin. Genet. Dev.* **17** 435–42
[2] Schermelleh L, Heintzmann R and Leonhardt H 2010 A guide to super-resolution fluorescence microscopy *J. Cell Biol.* **190** 165–75
[3] Huang B, Babcock H and Zhuang X 2010 Breaking the diffraction barrier: super-resolution imaging of cells *Cell* **143** 1047–58
[4] Llères D, James J, Swift S, Norman D G and Lamond A I 2009 Quantitative analysis of chromatin compaction in living cells using FLIM-FRET *J. Cell Biol.* **187** 481–96
[5] Llères D, Bailly A P, Perrin A, Norman D G, Xirodimas D P and Feil R 2017 Quantitative FLIM-FRET microscopy to monitor nanoscale chromatin compaction *in vivo* reveals structural roles of condensin complexes *Cell Rep.* **18** 1791–803
[6] Pelicci S, Diaspro A and Lanzanò L 2019 Chromatin nanoscale compaction in live cells visualized by acceptor-to-donor ratio corrected Förster resonance energy transfer between DNA dyes *J. Biophoton.* **12** e201900164
[7] Chatel G, Desai S H, Mattheyses A L, Powers M A and Fahrenkrog B 2012 Domain topology of nucleoporin Nup98 within the nuclear pore complex *J. Struct. Biol.* **177** 81–89
[8] Gustafsson M G L 2000 Surpassing the lateral resolution limit by a factor of two using structured illumination microscopy *J. Microsc.* **198** 82–87
[9] Markaki Y *et al* 2012 The potential of 3D-FISH and super-resolution structured illumination microscopy for studies of 3D nuclear architecture *BioEssays* **34** 412–26
[10] Betzig E *et al* 2006 Imaging intracellular fluorescent proteins at nanometer resolution *Science (80-.)* **313** 1642–6
[11] Ricci M A, Manzo C, Garcìa-Parajo M F, Lakadamyali M and Cosma M P 2015 Chromatin fibers are formed by heterogeneous groups of nucleosomes *in vivo Cell* **160** 1145–58
[12] Hell S W and Wichmann J 1994 Breaking the diffraction resolution limit by stimulated emission depletion fluorescence microscopy *Opt. Lett.* **19** 780–2
[13] Mitchell-Jordan S, Chen H, Franklin S, Stefani E, Bentolila L A and Vondriska T M 2012 Features of endogenous cardiomyocyte chromatin revealed by super-resolution STED microscopy *J. Mol. Cell. Cardiol.* **53** 552–8
[14] Cseresnyes Z, Schwarz U and Green C M 2009 Analysis of replication factories in human cells by super-resolution light microscopy *BMC Cell Biol.* **12** 1–12
[15] Schermelleh L *et al* 2008 Subdiffraction multicolor imaging of the nuclear periphery with 3D structured illumination microscopy *Science* **320** 1332–6
[16] Löschberger A *et al* 2012 Super-resolution imaging visualizes the eightfold symmetry of gp210 proteins around the nuclear pore complex and resolves the central channel with nanometer resolution *J. Cell Sci.* **125** 570–5
[17] Gao M *et al* 2018 Expansion stimulated emission depletion microscopy (ExSTED) *ACS Nano* **12** 4178–85
[18] Pesce L, Cozzolino M, Lanzanò L, Diaspro A and Bianchini P 2019 Measuring expansion from macro- to nanoscale using NPC as intrinsic reporter *J. Biophoton.* **12** e201900018

[19] Vicidomini G *et al* 2011 Sharper low-power STED nanoscopy by time gating *Nat. Methods* **8** 571
[20] Tortarolo G, Sun Y, Teng W, Ishitsuka Y and Vicidomini G 2019 Nanoscale photon-separation to enhance the spatial resolution of pulsed STED microscopy *Nanoscale* **11** 1754–61
[21] Vicidomini G *et al* 2013 STED nanoscopy with time-gated detection: theoretical and experimental aspects *PLoS One* **8** e54421
[22] Lanzanò L, Coto Hernández I, Castello M, Gratton E, Diaspro A and Vicidomini G 2015 Encoding and decoding spatio-temporal information for super-resolution microscopy *Nat. Commun.* **6** 6701
[23] Hernández I C *et al* 2019 Efficient two-photon excitation stimulated emission depletion nanoscope exploiting spatiotemporal information *Neurophotonics* **6** 1–8
[24] Lanzanò L *et al* 2017 Measurement of nanoscale three-dimensional diffusion in the interior of living cells by STED-FCS *Nat. Commun.* **8** 65
[25] Sarmento M J *et al* 2018 Exploiting the tunability of stimulated emission depletion microscopy for super-resolution imaging of nuclear structures *Nat. Commun.* **9** 1–11
[26] Diaspro A 2019 *Nanoscopy and Multidimensional Optical Fluorescence Microscopy* (Boca Raton, FL: Chapman and Hall/CRC)
[27] Harke B, Keller J, Ullal C K, Westphal V, Schönle A and Hell S W 2008 Resolution scaling in STED microscopy *Opt. Express* **16** 4154–62
[28] Tortarolo G, Castello M, Diaspro A, Koho S and Vicidomini G 2018 Evaluating image resolution in stimulated emission depletion microscopy *Optica* **5** 32–35
[29] Oneto M *et al* 2019 Nanoscale distribution of nuclear sites by super-resolved image cross-correlation spectroscopy *Biophys. J.* **117** 2054–65
[30] Enderlein J 2005 Breaking the diffraction limit with dynamic saturation optical microscopy *Appl. Phys. Lett.* **87** 94105